



# Mechanical Properties and Damage Behavior of Polypropylene Composite (GF50-PP) Plate Fabricated by Thermocompression Process Under High Strain Rate Loading at Room and Cryogenic Temperatures

Joseph Fitoussi<sup>1</sup> · Mohammad Hossein Nikooharf<sup>1</sup> · Achraf Kallel<sup>2</sup> · Mohammadali Shirinbayan<sup>1</sup>

Received: 3 February 2022 / Accepted: 17 June 2022 / Published online: 18 July 2022  
© The Author(s), under exclusive licence to Springer Nature B.V. 2022

## Abstract

This paper concerns the coupling effect of strain rate and temperature on the damage mechanical properties of the long-glass-fiber-reinforced polypropylene (GF50-PP) composite produced by the thermocompression process. Composite plates of GF50-PP have been employed to study the effect of glass fiber distribution on the mechanical properties of the composites. To achieve this objective the tensile tests have been performed at strain rate range from quasi-static to  $100 \text{ s}^{-1}$  at two loading temperatures of  $20 \text{ }^\circ\text{C}$  and  $-70 \text{ }^\circ\text{C}$ , while measuring the local deformation through a contactless technique using a high-speed camera. High strain rate tensile tests findings showed that GF50-PP behavior is strongly strain-rate dependent. For instance, the stress damage threshold for three fiber orientations of  $0^\circ$ ,  $45^\circ$ , and  $90^\circ$  to the Mold Flow Direction (MFD) was increased, when the strain rate varies from quasi-static ( $0.001 \text{ s}^{-1}$ ) to  $100 \text{ s}^{-1}$  at two loading temperatures of  $20 \text{ }^\circ\text{C}$  and  $-70 \text{ }^\circ\text{C}$ . The experimental methodology was coupled to microscopic observations using SEM to study the damage mechanisms of GF50-PP. The analysis confirms that there are three damage mechanisms: fiber-matrix interface debonding, matrix breakage, and pseudo-delamination between neighboring bundles of fibers.

**Keywords** Glass-fiber-reinforced polypropylene composite · Thermocompression · Cryogenic test · Strain rate · Fiber distribution

---

✉ Mohammadali Shirinbayan  
mohammadali.shirinbayan@ensam.eu

Joseph Fitoussi  
joseph.fitoussi@ensam.eu

Mohammad Hossein Nikooharf  
mohammad\_hossein.nikooharf\_tamiz@ensam.eu

Achraf Kallel  
achraf.kallel@devinci.fr

<sup>1</sup> Arts Et Metiers Institute of Technology, CNAM, PIMM, HESAM University, 75013 Paris, France

<sup>2</sup> Léonard de Vinci Pôle Universitaire, Research Center, La Défense, 92916 Paris, France

## 1 Introduction

Several studies have demonstrated that thermoplastic polymer-based composites offer advanced performance and properties such as good recyclability, low weight, low cost, high toughness and enhanced impact resistance [1–6]. Hence, they would promise a broad range of industrial applications, for instance in the aerospace, automotive, and petroleum industries [7–11].

The used composite consisted of polypropylene (PP) matrix reinforced with high strength glass fibers. The proposed material provides a good combination of high ductility of the matrix with high strength of load-bearing fibers. Eventually, this composite is widely used due to its advantageous processing characteristics and excellent physicochemical stability, as well as cost-effectiveness [12–16].

Glass-fiber-reinforced polypropylene (GFPP) composites have been widely used in transportation, automotive, and petroleum, marine and military applications [17–24] due to their elevated mechanical performance by virtue of their reliable strength, stiffness, impact properties; lightweight; fast and inexpensive production; and recyclability [20, 25–27].

Moreover, the GFPPs are increasingly used for insulation applications due to their chemical resistance, especially in acid/alkaline environments, high thermal decomposition temperature, creep resistance and high hydrophobicity [28].

Stiffness confinement effects, which occur close to rigid interfaces, improve the stiffness of composites by restricting the movement of polymer chains [29, 30]. It is also accepted that fibers can act as nucleating agents, triggering heterogeneous nucleation of polymer and interfacial crystallization on their surface by forming a transcrystalline layer nearby the fibers in the composites. These crystalline areas provide increased interfacial interaction between polymer and filler and improve the mechanical properties of the composites [31, 32].

Notwithstanding current advantages, the significant prospects of composite materials in the future industry inevitably give rise to concern. The hydrogen industry as a reliable source of energy would face the rise of several challenges, including in gas storage, transfer and application along with the other renewable energy sources. In this regard, polymer-based composites would play a promising role by providing reliable thermo-mechanical properties.

It is worth mentioning that by cooling the material down to the cryogenic temperature, unequal coefficients of thermal expansion between the fibers and the matrix would cause significant internal stresses that would eventually initiate the formation of microcracks in the polymer matrix [33, 34].

One can note that even though compressed gas and liquid hydrogen vessels generally operate at a constant temperature, cryo-compressed vessels would face significant pressure/temperature variations, depending on the gas discharge rate [35]. Consequently, with respect to the behavior of the stored fluid, a comprehensive understanding of the mechanical properties of vessel components under various stresses and temperatures in cryogenic conditions would be essential.

While the GFPP could be fabricated by employing different processing methods, the injection molding process is the most used production technic [36–39]. Since this process is suitable for the fabrication of short fiber composites, other techniques need to be investigated to produce long fiber-reinforced composites, concerning industrial applications notably the automotive sector. In this study, the thermo-compression molding

process has been employed as one of the most simple and cost-effective methods for large-scale processing of thermoplastic long fiber-reinforced composites [40–42].

The thermo-compression process composite sheets were manufactured by conventional thermal compression molding process by the following four steps (Fig. 1) according to the desired thermal curve processing cycle [42].

The process consists of heating fiber-reinforced thermoplastics above melting temperature to initiate the material flow followed by mold filling and thermo-compressing, in which the mold walls press the material into the mold. The cooling phase is the final step in product processing by thermo-compression molding [40–46].

The core element of the compression molding process is the mold filling, the moment when the fiber-reinforced material is placed into the mold and the closing mold walls force the material into the cavity under pressure. Mold filling is considered as one of the most important phases of the compression molding process, in which the fiber reinforced thermoplastic heated above the melting temperature is placed into the mold and the material is forced into the cavity under pressure [41]. This step would be followed by the cooling phase, in which the crystallization will occur and eventually complete the process [28, 31].

The composite mechanical properties depend on different process parameters such as fiber orientation and distribution, fiber length and fiber-matrix interface interactions. Consequently, although randomly oriented fiber meshes were used in process design, in this work, three different orientations ( $0^\circ$ ,  $45^\circ$ ,  $90^\circ$ ) with respect to the production orientation axis have been studied in order to evaluate the specimen's homogeneity.

Constitutive law as an important indicator of the mechanical properties has been investigated regarding different loading conditions including variations in strain rate, temperature and tensile orientation. In order to establish the relation between the GFPP composite mechanical properties and the thermo-compression molding process parameters, various experimental studies have been carried out using different specimens. Previous studies have already investigated the thermo-compression process parameters' impact on mechanical properties of GFPP such as the effect of cooling rate [47], mold pressure, mold temperature, and holding time [48]. Furthermore, other studies have been conducted to analyze the impact of the fiber properties such as porosity, fiber length, fiber relative fraction content and distribution on the mechanical properties of the GFPP [49, 50]. The fiber-matrix interface properties would play an important role in microstructural deformation mechanisms and eventual mechanical properties of long fiber-reinforced thermoplastics during compression molding, as reported in [41, 51, 52]. For instance, a numerical approach has been utilized in several studies in order to predict the fiber matrix separation during the compression molding process [52–54].

It can be concluded that the fiber interactions including fiber bridging and interlocking inside complex geometries could result in the fiber matrix separation, regarding

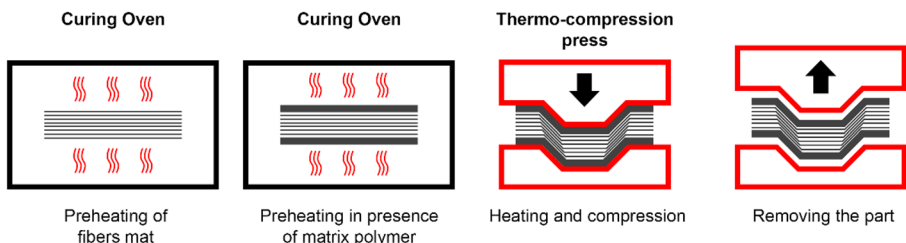


**Fig. 1** Conventional thermal compression moulding process of thermoplastic composites [42]

initial parameters such as fiber orientation, initial mold filling and the desired final geometry, which are among the most important parameters influencing the final fiber properties [10].

Constitutive law is considered an important indicator in order to achieve a structural design specially for complex geometries. Regarding this approach, a general comprehension of the material behavior in different temperature and loading conditions would be necessary.

Various studies have already established experimental and prediction models to better understand the constitutive law of GFPP under normal loading conditions [55–57]. Extent the behavior law under extreme loading conditions such as high strain rates and cryogenic environments still needed to be more investigated. Moreover, as gradual damage is believed to be one of the most critical failure mechanisms of composite materials, a profound damage study would be important to obtain a reliable behavior law modeling for composites [55]. Consequently, in this work one has investigated the experimental studies of damage behavior of GFPP as well as their behavior under extreme conditions (the strain rates up to  $1.15 \text{ m}\cdot\text{s}^{-1}$  and the temperature of  $-70 \text{ }^\circ\text{C}$ ), since the material would be used in the natural gas and hydrogen vessels storage applications.

In summary, obtaining desired functions of the processed products, a deep understanding and prediction capability of the process-related parameters would be crucial, regarding their structural, morphological and rheological characteristics [10].

The aim of this work is to follow the evolution of the mechanical characteristics such as Young's modulus, threshold stress and strain, failure stress and strain, at different strain rates for three sample orientations ( $0^\circ$ ,  $45^\circ$  and  $90^\circ$ ) and under different loading temperatures ( $+20 \text{ }^\circ\text{C}$  and  $-70 \text{ }^\circ\text{C}$ ). These experimentations can help to feed the predictive models in order to the design calculation for different structural parts. This paper is divided into four main sections. The first section illuminates the importance of the high strain rate tests at ambient and cryogenic conditions and provides a brief overview of the previous literature, concerning the important phenomena relating the mechanical properties of the polymer-based composite in high strain rate and cryogenic state. The second part examines the material, processing, and characterization methods of the samples. Obtained results have been presented and discussed in the following section. The last section provided a general conclusion and presented the following perspective for future works.

## 2 Material and Experimental Procedures

### 2.1 Long-Glass-Fiber-Reinforced Polypropylene (GF50-PP)

GF50-PP composite has been used for this study which was supplied by Quadrant Plastic Composites AG (Lenzburg, Switzerland). A glass fiber mat containing 4 cm-long randomly oriented fibers has been used as reinforcement with a final fiber weight fraction of 50%. The polypropylene-based composite plates were produced by the thermo-compression molding process obtaining a density of  $1.33 \text{ g}\cdot\text{cm}^{-3}$ . As introduced in the introduction section, the thermo-compression molding process consists of the flow of the multi-layer foam to fill the mold. Hence, as shown in the discussion section, the final microstructure of the glass mat layer can be observed as an assembly of clusters linked together by entanglement in needling zones.

## 2.2 Microstructural Characterizations

### 2.2.1 Microstructure Analysis

The glass fiber distribution has been observed employing ZEISS optical microscopy along different views relative to Mold Flow Direction (MFD). Furthermore, Scanning Electronic Microscopy (HITACHI 4800 SEM) has been conducted in order to study the composite microstructure.

X-ray microtomography was used to analyze the fiber orientation of the sample ( $1 \times 1 \times 3 \text{ cm}^3$ ) which was placed between the X-ray beam and the camera detector.

### 2.2.2 Ultrasonic Measurement

Using ultrasonic waves for characterizing the orientation distribution of the composite fibers is a method representing advanced benefits as it has been mentioned in the literature [58, 59]. Hence, this method has been employed to investigate the fiber bundles orientation distribution in the GFPP composite. The present work bears a close resemblance with the previous work of [58].

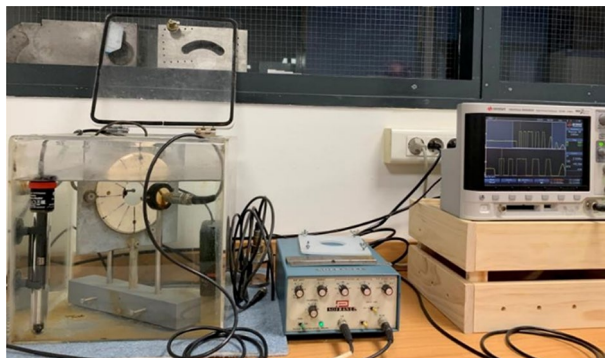
Figure 2 demonstrates the apparatus used for the ultrasonic test. The measurements method consisted of immersing equipment using two probes with a diameter of 10 mm, which perform as the transmitter and the receiver. The specimen was put between two probes with an angle of about  $45^\circ$  from the incident ultrasonic wave to generate a shear wave that propagates inside the material through a direction set on by applying the Snell-Descartes law [60].

According to [58], the ultrasonic shear stress was applied on the material in the plane defined by the incident wave and the vector normal to the plane of the specimen. By rotating the sample around the axis from  $0^\circ$  to  $360^\circ$ , the value of the shear waves velocity ( $V_{OT}$ ) is varied in line with the orientation distribution of the fibers. In conclusion, the ultrasonic measurement method can be considered a practical and convenient method since it is scanning a wide range of fiber orientations.

## 2.3 Thermo-mechanical Analysis

The thermo-mechanical behavior of the composite has been studied using Flexural dynamic mechanical tests by TA Instruments DMA Q800 in order to measure the main

**Fig. 2** Ultrasonic measurement apparatus



transition temperatures as well as loss, storage and complex moduli. The flexural test has been conducted at a temperature ranging from  $-70$  to  $140$  °C, a heating rate of  $3$  °C•min<sup>-1</sup> and a flexural frequency of  $1$  Hz applying a strain of  $0.1\%$ .

## 2.4 Mechanical Characterization

### 2.4.1 Quasi-static Tensile Test

The INSTRON 5966 machine has been used to perform the quasi-static tensile experimental tests, by applying a displacement rate of  $5$  mm•min<sup>-1</sup> and using a  $10$  kN load cell. Three fiber orientations of  $0^\circ$  (parallel to MFD),  $45^\circ$  and  $90^\circ$  (perpendicular to MFD) have been studied by the tensile test. At least five samples were carried out in order to confirm the reproducibility and to guarantee a favorable accuracy of the results.

### 2.4.2 High Strain Rate Tensile Test

A servo-hydraulic testing machine "Schenk Hydropuls VHS 5020" was used to perform the high-strain rate tensile tests, capable of applying a range of crosshead speeds from  $0.1$  mm/s (quasi-static) to  $20$  m/s.

As illustrated in Fig. 3, the specimen is situated between the upper fixture containing the fixed grip and the load cell, and the lower moving fixture device. The piezoelectric crystal load cell with a capacity of  $50$  kN records the load applied during the test. Simultaneously, a non-contact measurement technique with a high-speed camera "FASTCAM-APX RS" with a frame rate of  $250,000$  frames per second has been employed to monitor the local deformation. The deformation has been measured according to the initial gauge length defined by two points marked on the surface of the specimens. Hence, image analysis would allow us to track the displacement of the centroid of each marked point during the test in order to measure the evolution of the strain as a function of time.

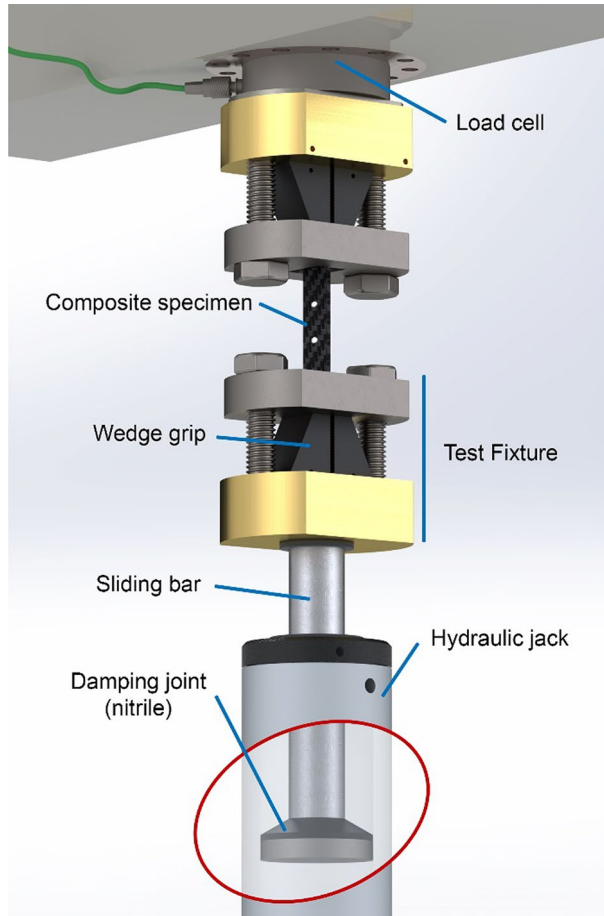
Load measurement under rapid dynamic conditions is subject to significant concerns due to signal disturbances, especially caused by system vibrations, which could become much more severe at higher strain rates [61]. In order to address this concern, the present work utilized the methodology previously developed by Fitoussi et al. [62], where a  $1.5$  mm "rubber nitride" damping layer was introduced as a "damping joint" at the interface of the slack adaptor and the hydraulic cylinder.

It can be noted that assuming the damping step represents a gradual increase in strain rate, the actual overall strain rate can be determined by considering the slope of the linear portion of the curve.

### 2.4.3 Damage Analysis

Damage analysis has been performed with three-points flexion tests by using a micro-machine situated inside an SEM chamber (HITACHI 4800 SEM). On account of the  $28$  mm span length of the machine, maximum travel of  $20$  mm at a rate of  $0.5$  mm/min has been applied to the center of the specimen (width:  $5.2$  mm and thickness:  $1.9$  mm).

**Fig. 3** The experimental device used for high-speed tensile tests



### 3 Experimental Results and Discussion

#### 3.1 Microstructural Evaluations

##### 3.1.1 Micrography Analysis

By Image analysis of the GF50-PP micrographs, a diameter of approximately  $15\ \mu\text{m}$  and a length of 4 cm for the glass fibers have been observable. Figure 4a represents an SEM micrograph of the GF50-PP sample. It is showing the randomly oriented bundle of fibers with a minor tendency to MFD orientation in some areas for the long glass fibers. In thermo-compression, the “multi-layer foam” is exposed to a flow allowing the mold to be filled. The microstructure of the glass mat layer can be presented as an assembly of clusters linked together by entanglement at the location of the needling zones (Fig. 4b). One can note that polypropylene can flow easily in needling zones constitute “pits”. This phenomenon can cause disentanglement during creep under the influence of local pressure. These analyses show the specific microstructure of the GF50-PP composite.

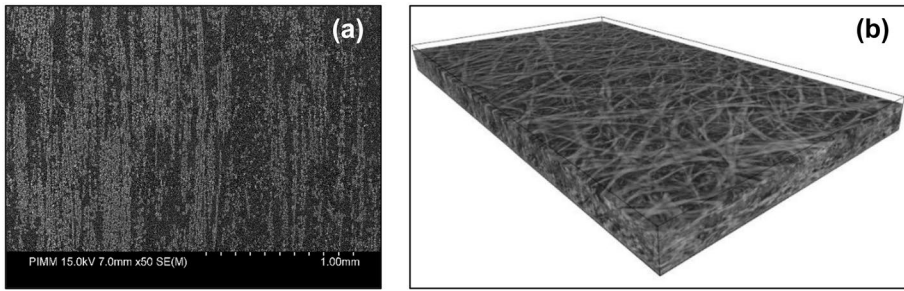


**Fig. 4** a Microstructure of GF50-PP in parallel to MFD view: Bundle of fibers and b 3d visualization

### 3.1.2 Ultrasonic Analysis

As mentioned before, shear wave velocity has been used as an indicator of the internal homogeneity of the sample and potential preferential fibers orientation. One can note that the almost circular polar diagrams for the majority of samples, illustrated in Fig. 5, demonstrate no preferred orientation of fibers. Consequently, the microstructure of the composite can be considered homogeneous. However, the two samples indicated as numbers 1 and 24 located at the edges of the composite plate present a preferred fibers orientation of  $330^\circ$ , with a  $30^\circ$  deviation from the MFD. The acoustical birefringence, coefficient  $K$  (%), is used to compare fiber orientation intensity and their distribution. This coefficient as mentioned in [58] can be defined as a variation function of the shear waves velocity as follows:

$$K(\%) = 100\% \times (V_{OT\max} - V_{OT\min}) / V_{OT\text{average}} \quad (1)$$

In which  $V_{OT}$  presents the velocity of the shear waves for a given relative orientation of the composite. As a result, higher values of  $K$  indicate the predominant orientation of fibers. Moreover, in terms of the spatial distribution of the fibers, high values of density, tensile and shear wave velocities demonstrate the presence of many fibers at the test location. One can note that the sampling has been done from the center of the plates.

### 3.2 Thermo-mechanical Analysis

The DMTA test has been performed to determine the thermal behavior and the main transition temperatures of the GFPP composite. A strain of 0.01%, a frequency of 1 Hz, and a temperature range of  $-70^\circ\text{C}$  to  $140^\circ\text{C}$  were applied to dual cantilever samples.

Figure 6a represents the evolution of both storage and loss moduli of GFPP composite as a function of temperature, and Fig. 6b illustrates the damping factor ( $\tan \delta$ ) versus temperature. The peaks on this curve give directly the values of  $T_\alpha$  and  $T_\beta$  which correspond to the glass transition and the  $\beta$ -transition temperature respectively. According to the curve, a local maximum value of 0.0409 for  $\tan \delta$  has been observed in  $11.33^\circ\text{C}$ , which can be considered as the peak of the  $T_\alpha$  zone (glassy-rubbery state transition zone).

According to Fig. 6b, the second transition point,  $T_\beta$ , has been observed at  $75.29^\circ\text{C}$ . It can be assumed that the  $\beta$ -transition temperature  $T_\beta$  represents a light brittle-ductile



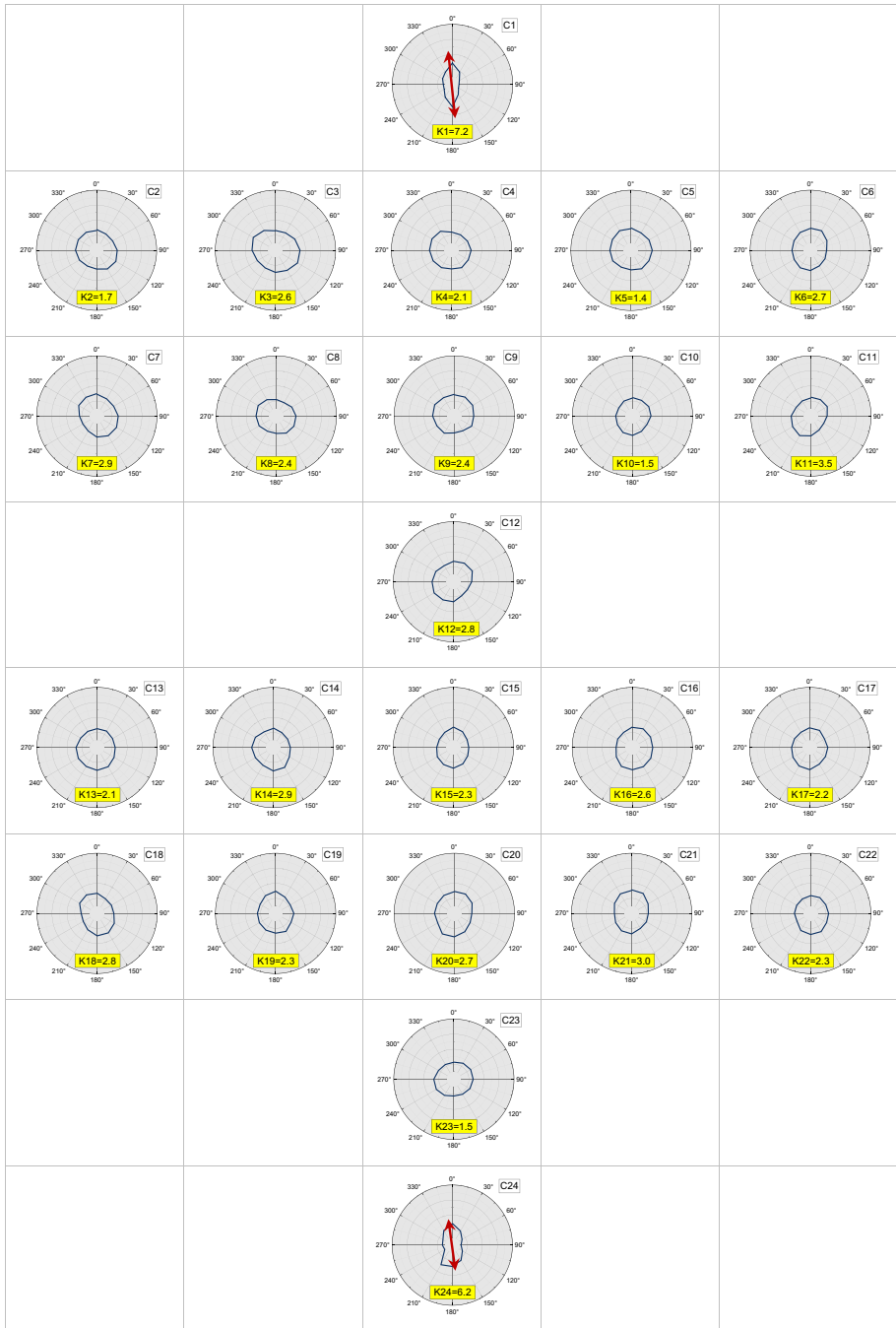
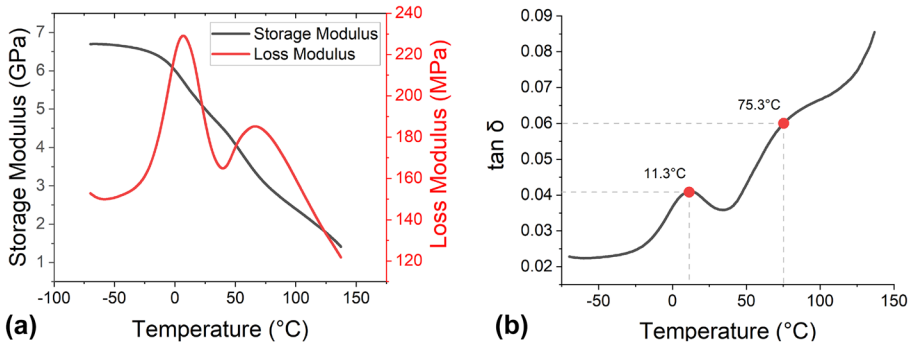


Fig. 5 Ultrasonic results of the GF50-PP composite plate, schematizing the sampling positions



**Fig. 6** DMTA test result: **a** evolution of the storage and loss moduli versus temperature, and **b** evolution of the  $\tan \delta$  versus temperature

transition in the matrix, mainly due to the stiffening of the polymer molecular chain segments located at the crystalline-amorphous interfaces and/or at the fiber-matrix interfaces [63].

The storage modulus decreased from 6695 MPa at -70 °C to 5188 MPa at 20 °C and eventually to 1410 MPa at 140 °C. This modulus experienced a smooth trend from the -70 °C until approximately -10 °C where it arrived at 6312 MPa, then decreased sharply by an almost linear trend to the end of the experiment. By increasing the temperature, molecular chain mobility would increase which declined proportionally the storage modulus.

The correlation of data from thermo-mechanical (DMTA) flexural test to linear data from quasi-static mechanical testing is achievable. As beta transition occurred at about 6.6 °C is related to the toughness of polymers, it is important to analyze the quasi-static behavior of the composite at the two temperatures of -70 °C and 20 °C.

### 3.3 Strain and Strain Rate Measurements

The high-speed tensile test was performed at a specified imposed velocity, whereas the actual strain rate ( $\dot{\epsilon}$ ) would be evaluated by further analysis of the deformation by image processing of the specimen during the tensile test. Figure 7 shows the examples of strain

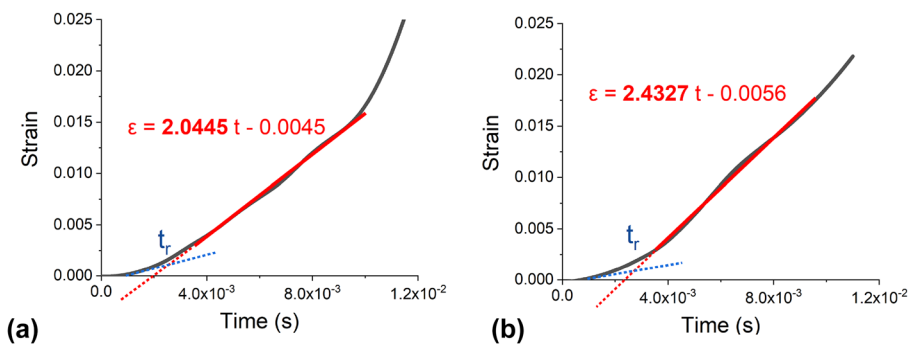


**Fig. 7** Strain rate measurement for two tensile test samples with an imposed velocity of 115 mm/s: **a** -70 °C and **b** +20 °C

evolution during a 115 mm/s-imposed velocity tensile test. For instance, as shown in Fig. 7a strain rate became steady after a gradual rise time for about 4 ms, and a constant strain rate is observable. By calculating the slope of the linear part for this sample, a strain rate of approximately  $2.044 \text{ s}^{-1}$  has been achieved for two thermal conditions. The obtained constant strain rate confirms the methodology of geometry calculation which has been presented in our previous works [63].

### 3.4 Quasi-static Tensile Results

To understand the mechanical behavior of the GF50-PP composite, the influence of the fiber orientation, temperature and strain rate and their accordance with the microstructural and thermal analyses has been investigated.

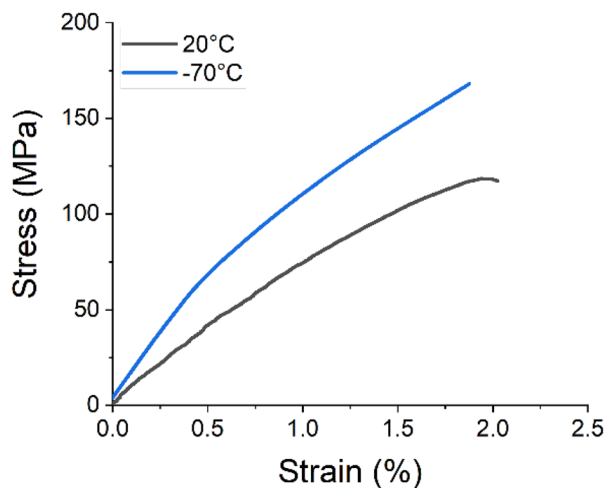
The results of the quasi-static tensile tests would provide the necessary data for the initial analysis of the mechanical behavior of the samples and their evolution as a function of the different fiber orientations and thermal conditions. In the following sections, the effects of strain rate on the specimens will be considered in order to obtain an overall view of the mechanical behavior.

#### 3.4.1 Effect of Loading Temperature

According to DMA results, polypropylene, having a glass transition temperature of about  $6.6 \text{ }^\circ\text{C}$ . This polymer exhibits a very temperature-sensitive behavior in several service environments.

In general, a significant difference in the quasi-static tensile behavior of GF50-PP samples at different temperatures has been observed. For instance, Fig. 8 provides a comparison of tensile behavior of GF50-PP  $45^\circ$  samples in quasi-static conditions at ambient and cryogenic temperatures. In this curve, higher stiffness and maximum strength are observable under cryogenic conditions compared to ambient temperature. One can see the failure stress at loading temperature of  $20 \text{ }^\circ\text{C}$  is about 115 MPa, however, this value is increased to 170 MPa, which is about 47%. The latter is related to the low molecular mobility at cryogenic conditions which increase the stiffness of the

**Fig. 8** Temperature effect on the mechanical behavior of GF50-PP samples during the quasi-static tensile test: an example of the tensile curve in two different temperatures for GF50-PP- $45^\circ$  sample



sample. However, the failure strain doesn't decrease as expected for the test at cryogenic temperatures. This trend can be related to the specific microstructure of the GF50-PP composite (see Fig. 4).

### 3.4.2 Effect of Fiber Orientation

The fabrication process introduces a variety of fiber orientation and distribution properties which would lead to complex microstructural interactions and slightly different overall properties [64]. Considering the dominant failure mechanisms of GFPP composites, including gradual fiber damage and breakage, fiber/matrix delamination, and eventual crack growth within the matrix, it is worth mentioning that slight differences in fiber distribution would lead to stochastic stress concentrations during deformation. These stress concentrations are dependent on deformation rate and temperature with respect to the viscoelastic behavior of the matrix, fiber elasticity, and fiber-matrix interface properties. Considering these uncertainties imposed by the fabrication process and environmental conditions, likewise the not fully random orientation tendencies within the ultrasonic results, slight variations in the macroscale mechanical behavior of the samples are to be expected.

Nevertheless, comparing the tensile results categorized by their sample orientations relative to the MFD would indicate orientation-dependent aspects affecting the macroscale behavior of composite. The quasi-static tensile results for samples with different fiber orientations have been compared in Fig. 9.

According to Fig. 9a, a slight difference in Young's modulus is observable at ambient temperature, while there is no noticeable difference observable in the stiffness of cryogenic samples (Fig. 9b). This phenomenon represents the effect of matrix rigidity on the load-bearing portion of the fibers in the elastic stage, where the rubbery matrix allows the fibers to reconfigure slightly in response to the applied stress and to have orientation-dependent behaviors emerged. On the other hand, the glassy matrix limited the effect of fiber configurational properties on the overall stiffness of the composite at cryogenic temperatures. This difference is also discussed in the following chapter of "Effect of strain rate on threshold and failure stress/strain".

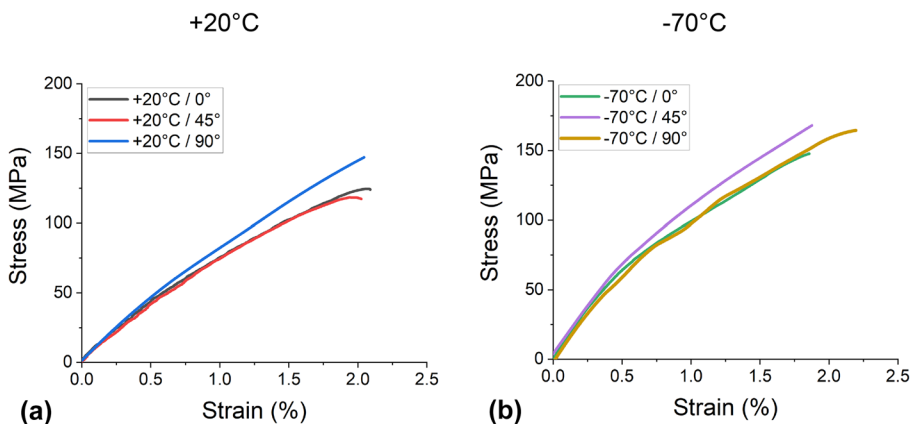


**Fig. 9** Tensile results comparison for different fiber orientations at **a** ambient and **b** cryogenic temperatures

### 3.5 High Strain Rate Tensile Results

To study the effect of fiber orientation, temperature, and strain rate on the mechanical behavior of the GF50-PP composite, several uniaxial tensile tests have been performed on three different sample orientations. These studies would eventually provide the necessary data, such as Young's modulus and threshold and ultimate stresses as the functions of temperature and strain rate, to model the behavior law of the composite. GF50-PP composite would be employed in hydrogen or gas reservoirs used for automotive and civil applications which must comply with strict safety standards, such as crash tests. Considering severe conditions of crash events, a profound study of the high strain rate behavior of these composites would be necessary.

Figure 10 provides a comparison of some of the tensile results at different strain rates. Non-elastic deformation of composite is assumed to be a combination of visco-plastic deformation of the matrix polymer and irreversible microstructural damages of composite. The latter can be considered as the dominant phenomenon, regarding the low plastic deformation capacity of the fibers and the low elongation at failure of the composite due to the early initiation of failure mechanisms. The damage initiation can be spotted as a knee point, ending the linear elastic stage, followed by a nearly linear deformation concerning the damage propagation stage [55, 56].

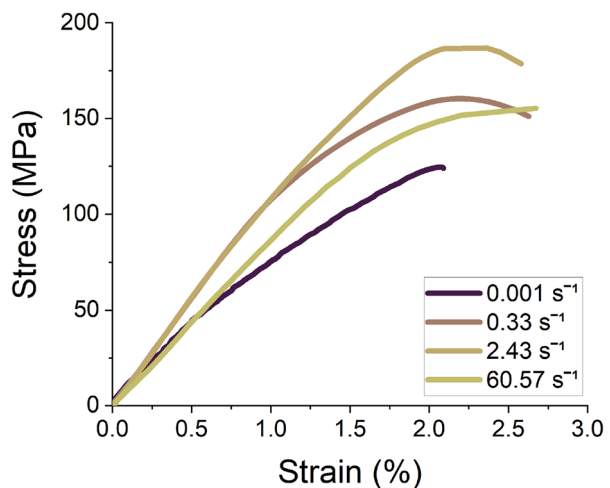
### 3.6 Effects of Strain-rate on the Overall Tensile Response

Strain rate has various influences on the threshold and the failure stress and strain results. To acquire an overall understanding of the influence of strain rate on the tensile response of the composite, a detailed analysis of the influences of temperature and the fiber orientation under different conditions would be necessary.

#### 3.6.1 Young Modulus Evolutions

Not surprisingly, Young's modulus values remain insensitive to strain rate, although temperature and orientation have been observed to affect the stiffness of the samples. As

**Fig. 10** Strain rate effect on tensile curves at 20 °C for a sample with fiber orientation of 90°



demonstrated in Fig. 11, cryogenic temperature samples exhibit higher stiffness for all strain rates and fiber orientations. A dependency of Young's modulus on fiber orientation and strain rate is observed at room temperature. Although there is no significant difference observable between the results obtained from different fiber orientations at cryogenic temperature. One can notice that tensile testing at a temperature above the glass transition temperature would result in different fiber-matrix decohesion during damage and fracture mode. Considering the stiffness, during the ambient temperature tensile test, the load-bearing portion of the fibers in the composite could be more prominent due to the rubbery intrinsic nature of the matrix. Thus, the overall stiffness is more dependent on the fiber conditions compared to the cryogenic testing.

### 3.6.2 Effect of Strain Rate on Threshold and Failure Stress/Strain

Figures 12 and 13 demonstrate an overall view of the influence of the strain rate on the threshold and failure properties, respectively. As stated before, the tensile properties of the GF50-PP composite dominantly depend on damage initiation and propagation. Accordingly, one can assume that specifically under low temperature and high strain-rate conditions, the threshold strength is controlled by the damage mechanisms. Subsequently, one can note that the low-temperature results would be much more sensitive to the strain rates and fiber orientation. From an overall view of Fig. 12, one can note that the threshold is increased by raising the strain rate in almost all fiber orientations and temperatures. The significant strain rate dependence of the threshold strength (knee point) would ascertain the viscous nature of damage mechanisms [56], indicating a delay in damage initiation by increasing the strain rate. Contrary to the stiffness results, fiber conditions would have an important effect on the threshold strength at low temperatures and high strain rates. Overall, for most of the samples, the cryogenic tests exhibited higher threshold stress and slightly lower threshold strain results. At cryogenic temperatures, samples perpendicular to the MFD show higher threshold stress results in rapid dynamics compared to the other directions, as well as ambient temperature results of the same samples. Nonetheless, in the quasi-static state, the temperature has had no significant influence on the threshold strength of these samples, and their results show even lower strengths compared to samples from other directions. On the other hand, samples oriented at 45° to the MFD behave in a reverse manner to the perpendicular samples in the cryogenic state. They show the slight

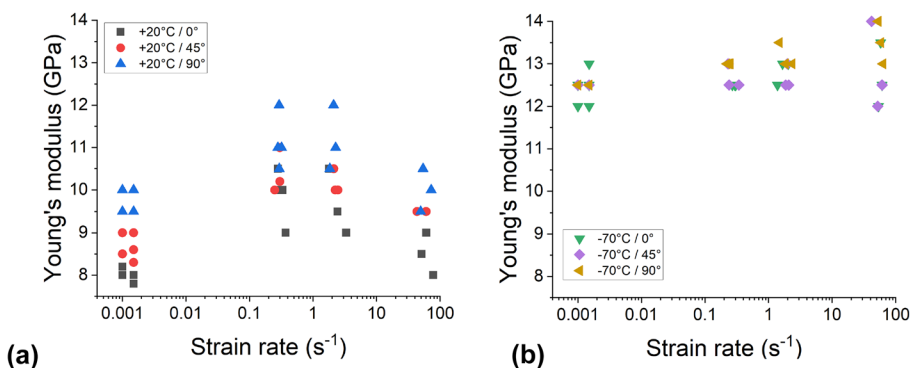


**Fig. 11** Evolution of Young's modulus versus the strain rate at **a** 20 °C and **b** -70 °C

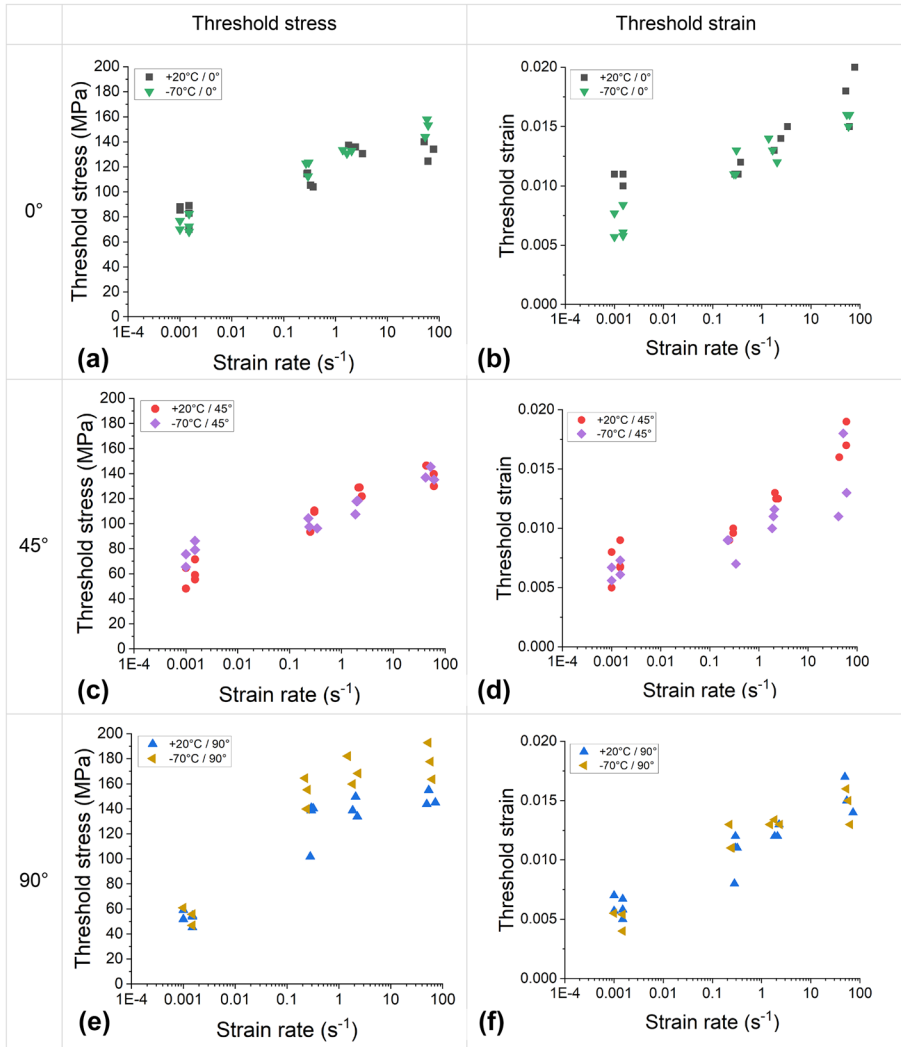


**Fig. 12** Evolution of the threshold stress/strain versus strain rate **a, b** 0°, **c, d** 45° and **e, f** 90 °C

lowest threshold strength results in rapid dynamics compared to the other direction results. Although they have shown slightly higher threshold strength in the quasi-static state compared to other directions as well as ambient temperature results of the same samples.

Furthermore, it can be noted that for the 45° samples, in contrast to the parallel and perpendicular samples, the cryogenic threshold strength results demonstrate a slight dependence on the strain rate, in comparison to ambient temperature results. The threshold strain results show various trends against strain rate variations for different fiber orientations and testing temperatures. However, it can be stated that the ambient temperature results present a slightly higher variation compared to the cryogenic results for the same sample conditions. At ambient temperature, the samples oriented parallel to the MFD direction exhibit slightly higher elongation compared to the almost identical results for the 45- and

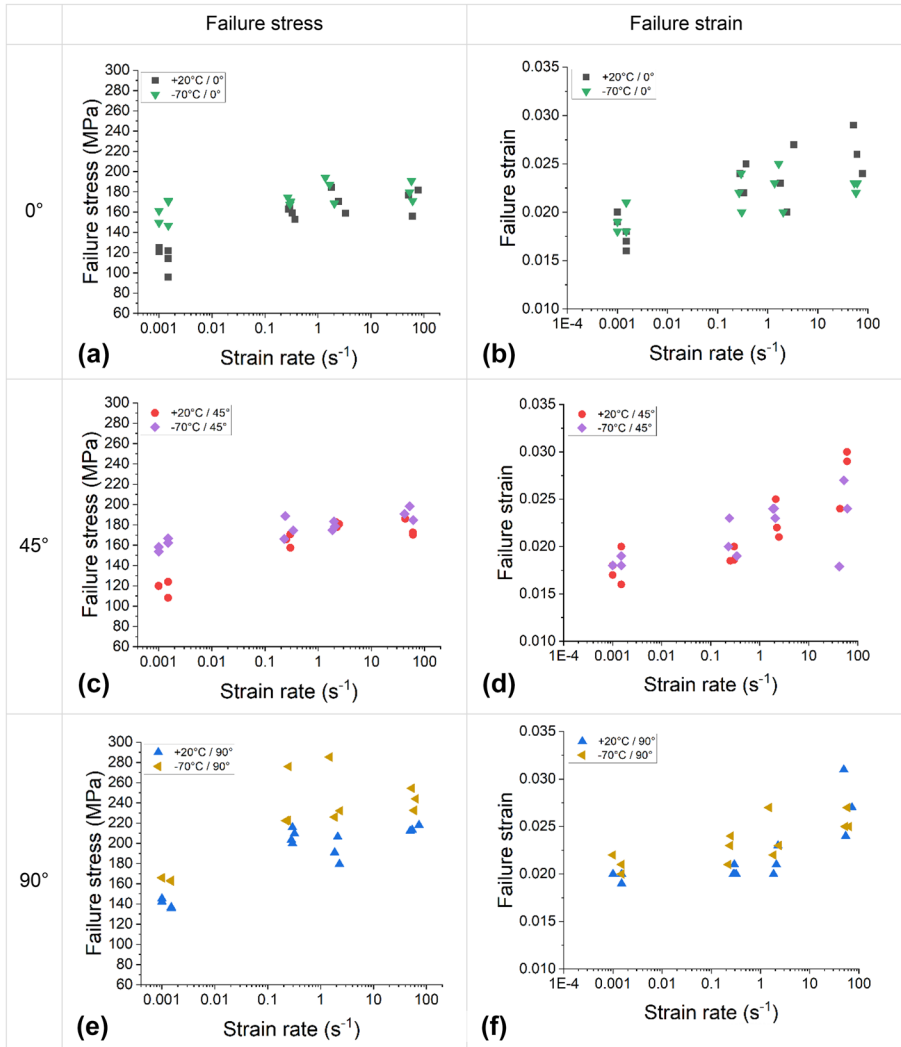


**Fig. 13** Evolution of the failure stress/strain versus strain rate **a, b** 0°, **c, d** 45° and **e, f** 90 °C

90-degree samples. This phenomenon is especially more significant at lower strain rates since there is clear diversity in the quasi-static results.

On the other hand, at cryogenic temperatures, the threshold strain of different orientations is ordered differently in quasi-static and dynamic states. While in quasi-static states, the 0°, 45° and 90° samples show the highest to lowest threshold strain results, respectively. The 45-degree samples present the lowest results in rapid dynamics in comparison to other orientations.

In addition, samples of different orientations have demonstrated different dependency of threshold strain on strain rate in different testing temperatures. For perpendicular samples in rapid dynamics, there is no significant difference in the threshold strain values and in the dependence of the threshold strain on the strain rate, either at ambient or cryogenic



temperatures. While in the quasi-static state, a slight diversity can be observed, representing slightly higher values for the ambient temperature results. The 45-degree samples on the other hand demonstrate stronger dependence of threshold strain on the strain rate at ambient temperature compared to the cryogenic state. While there is no significant difference observable in the threshold strain in the quasi-static state. For the perpendicular samples on the other side, there is a clear diversion of results in the quasi-static state, which vanished by increasing the strain rate. Although the ambient temperature threshold strain can be considered higher than the cryogenic threshold strain at each strain rate.

In addition, one can see from Fig. 13 that for all microstructure orientation and temperatures, the failure stress/strain values are influenced by strain rate. For example, for the fiber orientation of  $90^\circ$  the failure stress is increased about 51% and 53% for two loading temperatures of  $20^\circ\text{C}$  and  $-70^\circ\text{C}$  by changing the loading rate from quasi-static to  $100\text{ s}^{-1}$ . This confirms that the effect of strain rate on failure stress is similar for both thermal conditions. Moreover, failure stress is less influenced by the loading rate for the samples with fiber orientation of  $45^\circ$  at  $-70^\circ\text{C}$ . In fact, failure stress is increased by about 50% and 30% for two loading temperatures of  $20^\circ\text{C}$  and  $-70^\circ\text{C}$  by changing the loading rate from quasi-static to  $100\text{ s}^{-1}$ .

### 3.7 Multi-scale Damage Analysis: In-situ Bending Test

The damage evolution under the in-situ bending test for the three studied fiber orientations is demonstrated in Fig. 14. A three-points quasi-static ( $0.5\text{ mm/min}$ ) bending test was performed to highlight the influence of the microstructure on damage mechanisms occurring at the local scale.

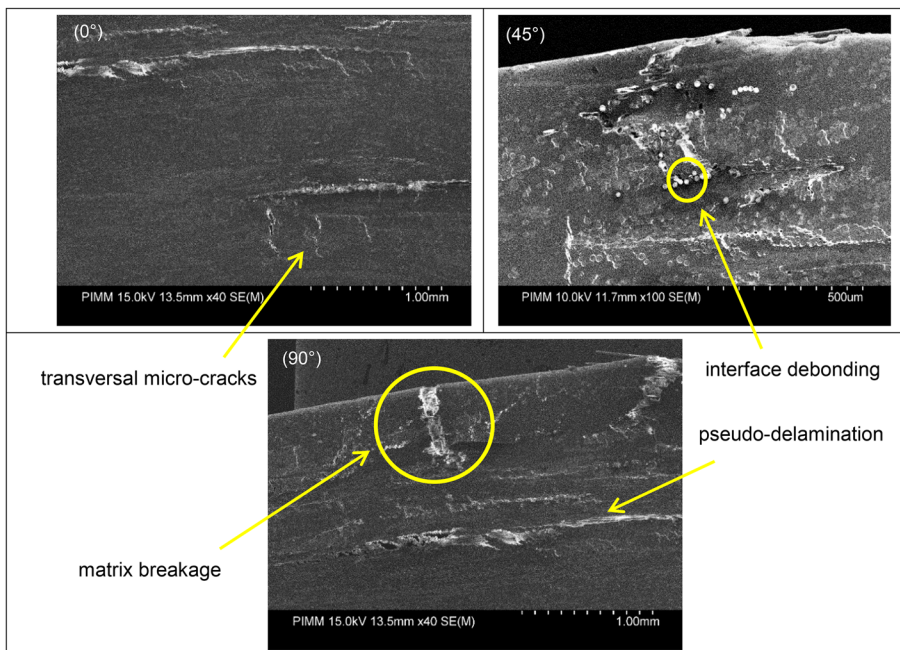


**Fig. 14** Microscopic failure images under bending test for three studied fiber orientations

One can see from these micrographs, for different fiber orientations, the main damage mechanisms belong to fiber-matrix interface debonding, matrix breakage and pseudo-delamination (just before failure). The presence of both pseudo-delamination between fibers and transversal micro-cracks emerged due to the combination of interface failure between adjacent fibers.

## 4 Conclusion

In this work, the coupling effect of strain rate and temperature on the damage mechanical properties of the long-glass-fiber-reinforced polypropylene (GF50-PP) composite produced by the thermocompression process has been studied. Since the material would be used in the natural gas and hydrogen vessels storage applications, a dynamic test with a high strain rate and at cryogenic conditions has been performed to better understand the behavior law of the GFPP composite. The microstructural analysis presented the particular microstructure of the GF50-PP. Polypropylene can flow easily in needling zones constitute "pits which can cause a disentanglement during creep under the influence of local pressure. So, the ultrasonic analysis was performed to specify the fiber orientation at different areas of the fabricated plates. A quasi-static tensile test was performed to study the mechanical behavior of the samples and their evolution as a function of the different orientations and temperature conditions. The tensile results showed the increase of the failure stress at loading temperature of  $-70\text{ }^{\circ}\text{C}$  due to the limited molecular mobility at cryogenic conditions. A small difference in Young's modulus is observable at ambient temperature ( $20\text{ }^{\circ}\text{C}$ ), while there is no noticeable difference observable in the stiffness of samples loaded at cryogenic conditions. The effect of the strain rate on the threshold and the failure stress and strain during the tensile response of the composite was carried out. The fiber orientations have an important effect on the threshold strength at low temperatures and high strain rates. In the cryogenic conditions, higher threshold stress and a slightly lower threshold strain were observed compared to results at the ambient temperature condition particularly for the samples perpendicular to the MFD. In addition, for all microstructure orientation and temperatures, the failure stress/strain values are increased by strain rate. Multi-scale damage analysis for different fiber orientations showed the main damage mechanisms belong to fiber-matrix interface debonding, matrix breakage and pseudo-delamination (just before failure).

**Data Availability** All data generated or analysed during this study are included in this published article.

## Declarations

**Ethical Approval** All procedures performed in studies were in accordance with the ethical standards of the institutional and/or national research committee.

**Consent to Participate** Not applicable.

**Consent to Publish** Not applicable.

**Conflict of Interest** The authors declare that they have no conflicts of interest.

## References

1. Yin, S., Tuladhar, R., Shi, F., Combe, M., Collister, T., Sivakugan, N.: Use of macro plastic fibres in concrete: A review. *Constr. Build. Mater.* **93**, 180–188 (2015). <https://doi.org/10.1016/j.conbuildmat.2015.05.105>
2. Cao, S., Yilmaz, E., Song, W.: Fiber type effect on strength, toughness and microstructure of early age cemented tailings backfill. *Constr. Build. Mater.* **223**, 44–54 (2019). <https://doi.org/10.1016/j.conbuildmat.2019.06.221>
3. Xue, G., Yilmaz, E., Song, W., Yilmaz, E.: Influence of fiber reinforcement on mechanical behavior and microstructural properties of cemented tailings backfill. *Constr. Build. Mater.* **213**, 275–285 (2019). <https://doi.org/10.1016/j.conbuildmat.2019.04.080>
4. Liu, J., Jia, Y., Wang, J.: Experimental study on mechanical and durability properties of glass and polypropylene fiber reinforced concrete. *Fibers and Polymers* **20**(9), 1900–1908 (2019). <https://doi.org/10.1007/s12221-019-1028-9>
5. Xu, L., et al.: Development of grid-reinforced carbon fiber mirrors using high-precision optical replication technology. *Opt. Eng.* **57**(9), 093110 (2018)
6. Al-darkazali, A., Çolak, P., Kadioğlu, K., Günaydın, E., Inanç, I., Demircan, Ö.: Mechanical properties of thermoplastic and thermoset composites reinforced with 3d biaxial warp-knitted fabrics. *Appl. Compos. Mater.* **25**(4), 939–951 (2018)
7. Asenjan, M.S., Sabet, S.A.R., Nekoomanesh, M.: Mechanical and high velocity impact performance of a hybrid long carbon/glass fiber/polypropylene thermoplastic composite. *Iran. Polym. J.* **29**(4), 301–307 (2020)
8. Gabr, M.H., Okumura, W., Ueda, H., Kuriyama, W., Uzawa, K., Kimpara, I.: Mechanical and thermal properties of carbon fiber/polypropylene composite filled with nano-clay. *Compos. B Eng.* **69**, 94–100 (2015)
9. Hassani, F., Martin, P.J., Falzo, B.G.: Progressive failure in interply hybrid composites of self-reinforced polypropylene and glass fibre. *Polymer* 122411 (2020)
10. Nikooharf, M.H., Rezaei-Khamesh, M., Shirinbayan, M., Fitoussi, J., Tcharkhtchi, A.: Comparison of the physicochemical, rheological, and mechanical properties of core and surface of polypropylene composite (GF50-PP) plate fabricated by thermocompression process. *Polym. Compos.* (2021)
11. Friedrich, K., Almajid, A.A.: Manufacturing aspects of advanced polymer composites for automotive applications. *Appl. Compos. Mater.* **20**(2), 107–128 (2013)
12. Huang, L., Wu, Q., Wang, Q., Wolcott, M.: Interfacial crystals morphology modification in cellulose fiber/polypropylene composite by mechanochemical method. *Compos. A Appl. Sci. Manuf.* **130**, 105765 (2020)
13. Gómez-Monterde, J., Sánchez-Soto, M., Maspoch, M.L.: Microcellular PP/GF composites: Morphological, mechanical and fracture characterization. *Compos. A Appl. Sci. Manuf.* **104**, 1–13 (2018)
14. Hamada, H., Fujihara, K., Harada, A.: The influence of sizing conditions on bending properties of continuous glass fiber reinforced polypropylene composites. *Compos. A Appl. Sci. Manuf.* **31**(9), 979–990 (2000)
15. Formisano, A., Papa, I., Lopresto, V., Langella, A.: Influence of the manufacturing technology on impact and flexural properties of GF/PP commingled twill fabric laminates. *J. Mater. Process. Technol.* **274**, 116275 (2019)
16. Díez-Pascual, A.M., Naffakh, M.: Polypropylene/glass fiber hierarchical composites incorporating inorganic fullerene-like nanoparticles for advanced technological applications. *ACS Appl. Mater. Interfaces.* **5**(19), 9691–9700 (2013)
17. Gu, S., Liu, H., Li, X., Mercier, C., Li, Y.: Interfacial designing of PP/GF composites by binary incorporation of MAH-g-PP and lithium bis (trifluoromethanesulfonyl) imide: towards high strength composites with excellent antistatic performance. *Compos. Sci. Technol.* **156**, 247–253 (2018)
18. Kim, D.-H., Kang, S.-Y., Kim, H.-J., Kim, H.-S.: Strain rate dependent mechanical behavior of glass fiber reinforced polypropylene composites and its effect on the performance of automotive bumper beam structure. *Compos. B Eng.* **166**, 483–496 (2019)
19. Kiss, P., Stadlbauer, W., Burgstaller, C., Archodoulaki, V.-M.: Development of high-performance glass fibre-polypropylene composite laminates: Effect of fibre sizing type and coupling agent concentration on mechanical properties. *Compos. A Appl. Sci. Manuf.* **138**, 106056 (2020)
20. Liu, Y., Deng, C.-L., Zhao, J., Wang, J.-S., Chen, L., Wang, Y.-Z.: An efficiently halogen-free flame-retardant long-glass-fiber-reinforced polypropylene system. *Polym. Degrad. Stab.* **96**(3), 363–370 (2011)

21. Yudhanto, A., et al.: Monotonic and cyclic responses of impact polypropylene and continuous glass fiber-reinforced impact polypropylene composites at different strain rates. *Polym. Testing* **51**, 93–100 (2016)
22. Arikan, V., Sayman, O.: Comparative study on repeated impact response of E-glass fiber reinforced polypropylene & epoxy matrix composites. *Compos. B Eng.* **83**, 1–6 (2015)
23. Chen, H., Wang, J., Ni, A., Ding, A., Sun, Z., Han, X.: Effect of novel intumescent flame retardant on mechanical and flame retardant properties of continuous glass fibre reinforced polypropylene composites. *Compos. Struct.* **203**, 894–902 (2018)
24. Duan, S., Zhang, Z., Wei, K., Wang, F., Han, X.: Theoretical study and physical tests of circular hole-edge stress concentration in long glass fiber reinforced polypropylene composite. *Compos. Struct.* **236**, 111884 (2020)
25. Kossentini Kallel, T., Taktak, R., Guermazi, N., Mnif, N.: Mechanical and structural properties of glass fiber-reinforced polypropylene (PPGF) composites. *Polym. Compos.* **39**(10), 3497–3508 (2018)
26. Liu, L., Liu, Y., Han, Y., Liu, Y., Wang, Q.: Interfacial charring method to overcome the wicking action in glass fiber-reinforced polypropylene composite. *Compos. Sci. Technol.* **121**, 9–15 (2015)
27. Varvani-Farahani, A.: Composite materials: characterization, fabrication and application-research challenges and directions. *Appl. Compos. Mater.* **17**(2), 63–67 (2010)
28. Wang, Y., Cheng, L., Cui, X., Guo, W.: Crystallization behavior and properties of glass fiber reinforced polypropylene composites. *Polymers* **11**(7), 1198 (2019)
29. Courtney, T.H.: *Mechanical behavior of materials*. Waveland Press (2005)
30. Krutyeva, M., et al.: Effect of nanoconfinement on polymer dynamics: surface layers and interphases. *Phys. Rev. Lett.* **110**(10), 108303 (2013)
31. Chen, Y., Wen, X., Nie, M., Wang, Q.: Preparation of polypropylene/glass fiber composite with high performance through interfacial crystallization. *J. Vinyl Add. Tech.* **23**(4), 284–289 (2017)
32. Karger-Kocsis, J., Czigány, T.: Interfacial effects on the dynamic mechanical behavior of weft-knitted glass fiber fabric-reinforced polypropylene composites produced of commingled yarns. Tensile and flexural response. *Appl. Compos. Mater.* **4**(4), 209–218 (1997)
33. Nobelen, M., Hayes, B.S., Seferis, J.C.: Cryogenic microcracking of rubber toughened composites. *Polym. Compos.* **24**(6), 723–730 (2003)
34. Kalia, S., Fu, S.-Y.: *Polymers at cryogenic temperatures*. Springer (2013)
35. Petitpas, G., Aceves, S.: Hydrogen storage in pressure vessels: liquid, cryogenic, and compressed gas. In: Klebanoff, L.E. (ed.) *Hydrogen Storage Technology: Materials and Applications*, pp. 91–107. CRC Press, Taylor & Francis (2012)
36. Yan, X., Uwongsuwan, P., Murakami, M., Imajo, A., Yang, Y., Hamada, H.: Tensile properties of glass fiber/carbon fiber reinforced polypropylene hybrid composites fabricated by direct fiber feeding injection molding process. In *ASME International Mechanical Engineering Congress and Exposition*, vol. 50527, p. V002T02A045. American Society of Mechanical Engineers (2016)
37. Yan, X., Yang, Y., Hamada, H.: Tensile properties of glass fiber reinforced polypropylene composite and its carbon fiber hybrid composite fabricated by direct fiber feeding injection molding process. *Polym. Compos.* **39**(10), 3564–3574 (2018)
38. Yu, L., Cui, Z.: Loading rate and temperature dependence of flexural behaviour of GFPP fabricated by Injection Molding Method
39. Yu, L., Ma, Y.: Loading rate and temperature dependence of flexural behavior in injection-molded glass fiber reinforced polypropylene composites. *Compos. B Eng.* **161**, 285–299 (2019)
40. Kim, D.-J., Yu, M.-H., Lim, J., Nam, B., Kim, H.-S.: Prediction of the mechanical behavior of fiber-reinforced composite structure considering its shear angle distribution generated during thermo-compression molding process. *Compos. Struct.* **220**, 441–450 (2019)
41. Kuhn, C.: Analysis and prediction of fiber matrix separation during compression molding of fiber reinforced plastics. (2018)
42. Antony, S., Cherouat, A., Montay, G.: Experimental investigation of the temperature effect on the mechanical properties of hemp woven fabrics reinforced polymer. *Appl. Mech.* **2**(2), 239–256 (2021)
43. Mülle, M., et al.: Process monitoring of glass reinforced polypropylene laminates using fiber Bragg gratings. *Compos. Sci. Technol.* **123**, 143–150 (2016)
44. Russo, P., Simeoli, G., Sorrentino, L., Iannace, S.: Effect of the compatibilizer content on the quasi-static and low velocity impact responses of glass woven fabric/polypropylene composites. *Polym. Compos.* **37**(8), 2452–2459 (2016)
45. Sorrentino, L., Simeoli, G., Iannace, S., Russo, P.: Mechanical performance optimization through interface strength gradation in PP/glass fibre reinforced composites. *Compos. B Eng.* **76**, 201–208 (2015)

46. Hoang, T.Q.T., Touchard, F.: Non-woven flax fibre reinforced polypropylene: Static and low velocity impact behaviour. *Polym. Polym. Compos.* **21**(5), 287–298 (2013)
47. Lee, I.-G., Kim, D.-H., Jung, K.-H., Kim, H.-J., Kim, H.-S.: Effect of the cooling rate on the mechanical properties of glass fiber reinforced thermoplastic composites. *Compos. Struct.* **177**, 28–37 (2017)
48. Kumar, B.S., Balachandar, S.: A study on the influence of hot press forming process parameters on Flexural Property of Glass/PP Based Thermoplastic Composites Using Box-Behnken Experimental Design. *Int. Sch. Res. Notices* **2014**, (2014)
49. Lekube, B.M., Hermann, W., Burgstaller, C.: Partially compacted polypropylene glass fiber non-woven composite: Influence of processing, porosity and fiber length on mechanical properties and modeling. *Compos. Part A: Appl. Sci. Manuf.* 105939 (2020)
50. Zhou, Y.G., Su, B., Turng, L.S.: Mechanical properties, fiber orientation, and length distribution of glass fiber-reinforced polypropylene parts: Influence of water-foaming technology. *Polym. Compos.* **39**(12), 4386–4399 (2018)
51. Dweib, M., Vahlund, C., Brádaigh, C.Ó.: Fibre structure and anisotropy of glass reinforced thermoplastics. *Compos. A Appl. Sci. Manuf.* **31**(3), 235–244 (2000)
52. Behrens, B.-A., Bohne, F., Lorenz, R., Arndt, H., Hübner, S., Micke-Camuz, M.: Numerical and experimental investigation of GMT compression molding and fiber displacement of UD-tape inserts. *Procedia Manuf* **47**, 11–16 (2020). <https://doi.org/10.1016/j.promfg.2020.04.109>
53. Park, C.H., Lee, W.I., Yoo, Y.E., Kim, E.G.: A study on fiber orientation in the compression molding of fiber reinforced polymer composite material. *J. Mater. Process. Technol.* **111**(1–3), 233–239 (2001). [https://doi.org/10.1016/s0924-0136\(01\)00523-4](https://doi.org/10.1016/s0924-0136(01)00523-4)
54. Londoño-Hurtado, A., Hernandez-Ortiz, J.P., Osswald, T.: Mechanism of fiber–matrix separation in ribbed compression molded parts. *Polym. Compos.* **28**(4), 451–457 (2007)
55. Notta-Cuvier, D., Nciri, M., Lauro, F., Chaari, F., Zouari, B., Maalej, Y.: A pragmatic approach for modelling the viscoelastic-viscoplastic behaviour of short-fibre reinforced thermoplastics coupled with anisotropic damage. *Appl. Compos. Mater.* **28**(2), 341–368 (2021)
56. Shirinbayan, M., Fitoussi, J., Meraghni, F., Surowiec, B., Bocquet, M., Tcharkhtchi, A.: High strain rate visco-damageable behavior of Advanced Sheet Molding Compound (A-SMC) under tension. *Compos. B Eng.* **82**, 30–41 (2015)
57. Shirinbayan, M., Fitoussi, J., Bocquet, M., Meraghni, F., Surowiec, B., Tcharkhtchi, A.: Multi-scale experimental investigation of the viscous nature of damage in Advanced Sheet Molding Compound (A-SMC) submitted to high strain rates. *Compos. B Eng.* **115**, 3–13 (2017)
58. Shirinbayan, M., Fitoussi, J., Abbasnezhad, N., Meraghni, F., Surowiec, B., Tcharkhtchi, A.: Mechanical characterization of a Low Density Sheet Molding Compound (LD-SMC): Multi-scale damage analysis and strain rate effect. *Compos. B Eng.* **131**, 8–20 (2017)
59. Schladitz, K., et al.: Non-destructive characterization of fiber orientation in reinforced SMC as input for simulation based design. *Compos. Struct.* **160**, 195–203 (2017). <https://doi.org/10.1016/j.compstruct.2016.10.019>
60. Zhang, S., Liu, L., Liu, Y.: Generalized laws of Snell, Fresnel and energy balance for a charged planar interface between lossy media. *J. Quant. Spectrosc. Radiat. Transfer* **245**, 106903 (2020)
61. Xiao, X.: Dynamic tensile testing of plastic materials. *Polym. Testing* **27**(2), 164–178 (2008)
62. Fitoussi, J., Meraghni, F., Jendli, Z., Hug, G., Baptiste, D.: Experimental methodology for high strain-rates tensile behaviour analysis of polymer matrix composites. *Compos. Sci. Technol.* **65**(14), 2174–2188 (2005)
63. Shirinbayan, M., Rezaei-khamseh, M., Nikooharf, M.H., Tcharkhtchi, A., Fitoussi, J.: Multi-scale analysis of mechanical properties and damage behavior of polypropylene composite (GF50-PP) plate at room and cryogenic temperatures. *Compos. Struct.* 114713 (2021)
64. Ghauch, Z.G., Aitharaju, V., Rodgers, W.R., Pasupuleti, P., Dereims, A., Ghanem, R.G.: Integrated stochastic analysis of fiber composites manufacturing using adapted polynomial chaos expansions. *Compos. A Appl. Sci. Manuf.* **118**, 179–193 (2019)